AIChE

Crystal Growth Rate Dispersion Modeling Using Morphological Population Balance

Cai Y. Ma and Xue Z. Wang
Institute of Particle Science and Engineering, School of Process, Environmental and Materials Engineering, University of Leeds, Leeds LS2 9JT, U.K.

DOI 10.1002/aic.11549
Published online July 10, 2008 in Wiley InterScience (www.interscience.wiley.com).

Crystal growth in solution is a surface-controlled process. The variation of growth rates of different crystal faces is considered to be due to the molecular arrangement in the crystal unit cell as well as the crystal surface structures of different faces. As a result, for some crystals, the growth rate for a specific facet is not only a function of supersaturation, but also dependent on some other factors such as its size and the lattice spread angle. This phenomenon of growth rate dispersion (GRD) or fluctuation has been described in literature to have attributed to the formation of some interesting and sophisticated crystal structures observed in experimental studies. In this article, GRD is introduced to a recently proposed morphological population balance model to simulate the dynamic evolution of crystal size distribution in each face direction for the crystallization of potash alum, a chemical that has been reported to show GRD phenomenon and sophisticated crystal structures. The GRD is modeled as a function of the effective relative supersaturation, which is directly related to crystal size, lattice spread angle, relative supersaturation, and solution temperature. The predicted results clearly demonstrated the significant effect of GRD on the shape evolution of the crystals. © 2008 American Institute of Chemical Engineers *AIChE J,* 54: 2321–2334, 2008
Keywords: growth rate dispersion, morphological population balance, morphology, crystal growth, shape, potash alum ($KAl(SO_4)_2 \cdot 12H_2O$)

Introduction

Crystals have regular internal arrangements of molecules in the asymmetric unit cell; therefore, they appear in specific shapes with multiple facets. It was known that the growth rates of individual faces vary and are strongly dependent on supersaturation.[1–3] For some compounds, studies on single crystals demonstrated that the growth rate of an individual face can also be dependent on its size, the lattice spread angle and some other factors. This phenomenon of growth rate dispersion (GRD) is considered to be responsible for some sophisticated and interesting crystal structures, such as the Christmas tree like structure of the crystals of potash alum, a typical compound exhibiting strong GRD.[1–8]

Population balance (PB) has been widely studied for modeling the evolution of crystal size distribution (CSD) in crystallizers, but traditionally the size of a crystal is defined as the diameter of a volume equivalent sphere, without taking into account the shape information. Obviously such an oversimplified definition for size is unable to simulate the crystal shape evolution of crystals in reactors. Recently multidimensional PB was proposed and investigated by several researchers,[9–14] and the majority of the work has been restricted to two-dimensions, e.g., the length and width of rode-like crystals and the face growth rates were correlated to supersaturation only. Doherty and coworkers[15] developed a new approach to combine a separate shape evolution model[16] with a standard one-dimensional PB model for the prediction of crystal shape evolution and applied the method to two-

Correspondence concerning this article should be addressed to X. Z. Wang at x.z.wang@leeds.ac.uk.

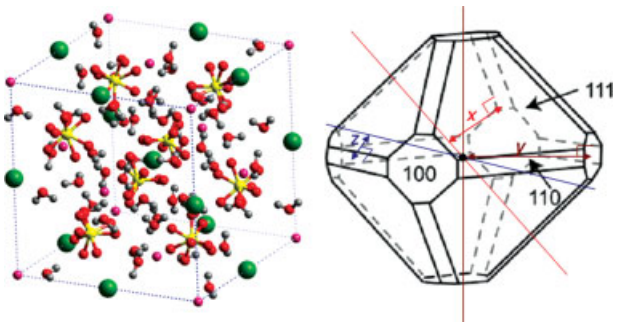

Figure 1. (Left) The molecular structure of potash alum ($KAl(SO_4)_2 \cdot 12H_2O$) with atom types being identified by color: K, green; Al, magenta; O, red; H, grey; S, yellow; (Right) The morphology of a potash alum crystal[1] and the schematic diagram of the three size characteristic parameters (*x*, *y*, *z*) to be used in a morphological population balance model for independent crystal faces.

dimensional tablet-like succinic acid crystals with fixed relative face growth rates. The shape evolution model[16] was further developed for the shape prediction of three-dimensional single crystals[17] and also for manipulation and simulation of crystal shape evolution during growth and/or dissolution.[18,19] In a recent study, we proposed a morphological PB model that can model more than two-dimensions,[20] in which the face growth rates were defined as functions of supersaturation. The purpose of the current study is to introduce GRD into the morphological PB model in order to simulate the sophisticated growth of crystals in a reactor that exhibit GRD. In the rest of the article, we will first introduce the GRD phenomenon for the model chemical, potash alum, then describe how GRD is incorporated into the morphological PB model in Morphological Population Balance Modeling of GRD section. Hot-Stage Experiment section briefly describes the hot-stage crystallisation experiment that generates data for comparison with simulation results. Detailed discussion of results will be given in Results and Discussions section, which is followed by conclusions in the final section.

GRD in Crystallization of Potash Alum

Potassium (potash) alum, $KAl(SO_4)_2 \cdot 12H_2O$, has four molecules in the cubic unit cell with space group of $Pa\bar{3}$ and cell parameters of $a = b = c = 12.517$ Å and $\alpha = \beta = \gamma = 90^\circ$ (see Figure 1, left side). Potash alum crystals can be easily grown from aqueous solutions and the morphology (Figure 1, right side) is dominated by the large octahedron face {111} and two essential but considerably smaller faces, the cubic face {100} and the rhomb-dodecahedron face {110}.[1,21] Figure 2 shows the molecular surface structures of potash alum crystals. It is clear that the distances of faces {100} and {110}, i.e., the distances between the dashed lines in Figure 2, are about 1.7 and 1.2 times larger than that for face {111}. According to the Bravais, Friedel, Donnay, and Harker[22–24] principle, the corresponding growth rates of faces {100} and {110} should be higher than that of face {111}.[2,25] In a study on a single potash alum crystal, GRD phenomenon for the {100} and {110} faces[1] was observed. The GRD is considered to be a key factor for the formation of defects and/or dislocations. The increase of growth rate was suspected to be due to the formation of a layer of small liquid inclusions on cube faces, which marks the position and shape of {100} face at the moment of the disturbance of growth conditions. As can be seen from Figure 2, the surface of face {100} presents more vacancies than the other two,

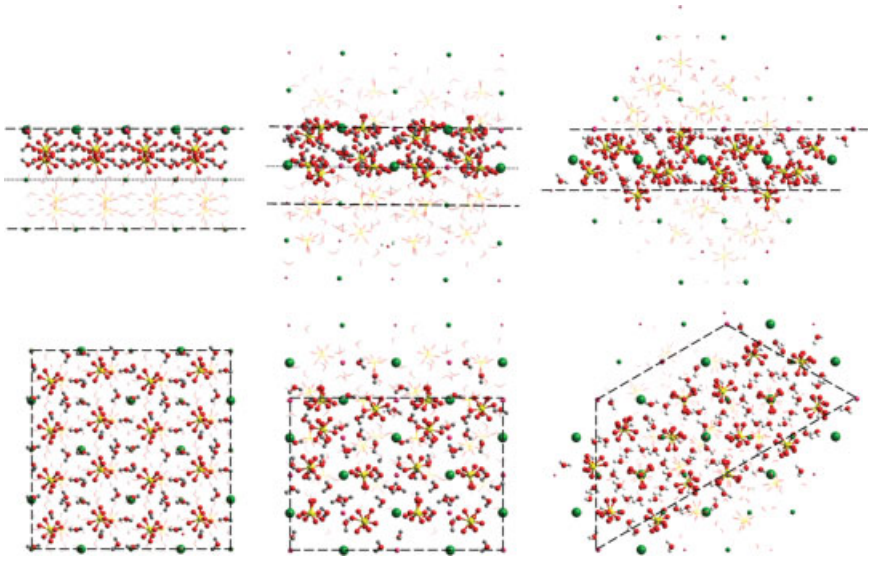

Figure 2. The molecular surface structures of a potash alum crystal with two views and each slab containing four unit cells: (left) {100} face; (middle) {110} face; (right) {111} face.

Atom types are colored as: K, green; Al, magenta; O, red; H, grey; S, yellow.

which can provide easier inclusion of water onto the surface of face {100}. Molecular dynamic simulation of potash alum crystal surfaces[26] indicated that the thickness of the flexible ions region for the surface of face {100} is larger than those for the other two. If two surfaces of face {100} attach to each other, a crystalline bridge can be easily formed without any rearrangement of ions or molecules because lateral movement of the two surfaces could form a perfect crystal structure,[26] which is a sign that water molecules may also be easily attached onto the surface of face {100}. After the formation of the water inclusions, the growth rate of the cube facet could be significantly increased; hence, resulting in smaller and smaller {100} face and eventually disappearing from the morphology. However, the fast growth of {100} face will slow down before the face vanishes completely, which will lead to increase in size for face {100} and the size of the face can return more or less to its former size. The decrease of growth rate could be caused by dislocations or strain, described by the mosaic structure of crystals, as was described in literature.[2,3,5,27–29] For small crystals, the extent of perfection of a crystal can be represented by a mosaic spread angle, η. The imperfect crystal structure will reduce the effective supersaturation during the crystal growth process.[5] For a crystal with edge length of L, there may exist many mosaic blocks with edge length of l_m. Between these mosaic blocks some small angle grain boundaries can be formed by the insertion of additional intermediate lattice planes, which forms edge dislocations. Therefore the mosaic blocks are tipped against each other by an angle θ, resulting in an enlargement of the measured mosaic spread angle, η. The grain boundary tension, γ_{gb}, can be calculated[3,5,27] by Eq. 1:

$$\gamma_{gb} = \frac{G_s b^* \eta}{4\pi(1-\nu)}\sqrt{\frac{l_m}{L}}\left[\frac{3}{4(1-\nu)} - \ln\left(4\pi\frac{r_c}{b^*}\right) + \ln\left(\frac{1}{\eta}\sqrt{\frac{L}{l_m}}\right)\right] \quad (1)$$

where G_s is the shear module, b^* is the length of the Burgers' vector, ν is the Poisson's ratio, and r_c is the radius of the dislocation center.

The energy per particle, E, due to the network of grain boundaries can be calculated by[3]

$$E = \gamma_{gb} A_{gb}\frac{\Omega}{L^3} = \frac{3G_s b^* \Omega}{4\pi(1-\nu)\sqrt{l_m}}\frac{\eta}{\sqrt{L}}\left[\frac{3}{4(1-\nu)} - \ln\left(4\pi\frac{r_c}{b^*}\right) + \ln\left(\frac{1}{\eta}\sqrt{\frac{L}{l_m}}\right)\right] \quad (2)$$

where Ω is the molecular volume, and A_{gb} is the total grain boundary area which can be approximated by

$$A_{gb} = 3L^2(L/l_m - 1) \approx 3L^3/l_m \quad (L >> l_m) \quad (3)$$

The effective relative supersaturation, σ_{eff}, can be written as[3,5]:

$$\sigma_{eff} = \sigma - \frac{E}{kT} = \sigma - \frac{3G_s b^* \Omega}{4\pi(1-\nu)kT\sqrt{l_m}}\frac{\eta}{\sqrt{L}} \times \left[\frac{3}{4(1-\nu)} - \ln\left(4\pi\frac{r_c}{b^*}\right) + \ln\left(\frac{1}{\eta}\sqrt{\frac{L}{l_m}}\right)\right] \quad (4)$$

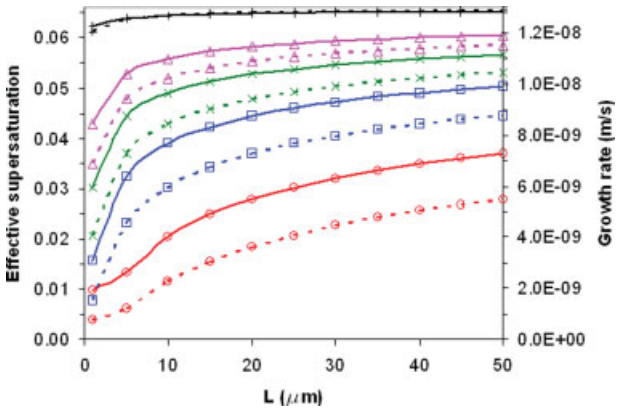

Figure 3. The variations of effective relative supersaturation (solid lines) and the corresponding growth rate (dotted lines) against crystal edge length, *L*, with different spread angle (η = 0.1 (+), 0.5 (△), 1.0 (×), 2.0 (□), 5.0° (○)) at a constant solution temperature.

[Color figure can be viewed in the online issue, which is available at www.interscience.wiley.com.]

where σ is the relative supersaturation calculated by ($C/C^* - 1$), k is the Boltzmann constant, and T is the temperature. The corresponding growth rate, G, is described as

$$G = k_0\,\sigma_{eff}^n \quad (5)$$

where k_0 is the growth kinetic coefficient and n is the order of kinetics. A similar method was used by Jones and Larson[30] to interpret the growth rate profiles of second nuclei of potash alum in single-crystal growth experiments with the BCF model of crystal growth.[31,32]

For potash alum crystals, the dependence of effective supersaturation on the crystal size and mosaic spread angle, with relative supersaturation of 0.0659 and temperature of 30°C, as being used in the experiments by Ristic et al.[2,28] and Sherwood and Ristic[29] is plotted in Figure 3 with the parameters in Eqs. 1–5 taken from literature.[3,5,27] The corresponding growth rate of {100} face using Eqs. 4 and 5 with $k_0 = 7.753 \times 10^{-7}$ m/s and $n = 1.5$ is also plotted in Figure 3. Figure 3 clearly shows the effect of crystal edge length and spread angle on crystal growth behavior, which is very similar to the results obtained by Lacmann et al.[5], Sherwood and Ristic,[29] and Jones and Larson.[30] The calculated grain boundary tensions under different mosaic spread angles decrease with the increase of crystal length, which has the same trend as obtained by Gerstlauer et al.[33] for the inner lattice strain under different crack efficiency of attrition.

It is worth mentioning that the term, GRD, was used to describe the growth phenomenon of faces {100} and {110}, in consistency with experimental studies in literature[1,3,5]. The equations describing GRD of these faces, Eqs. 1–4, have included their sizes, lattice spread angles and other factors.

Morphological Population Balance Modeling of GRD

A potash alum crystal has a total of 26 main habit faces[1,20] for which a geometric center can be found (Figure 1, right side). The normal distance of a crystal face to the geometric center forms one size dimension for a morphological PB model. In theory, a morphological PB model with 26 size dimensions is needed. In practice, if some faces, such as the eight {111} faces, are symmetry-related, suppose the symmetry-related faces have identical surrounding growth environment and hence same growth rates, these faces can be grouped into a single dimension (x) in the PB model. Similarly, the six {100} faces and 12 {110} faces will form the second size dimension, y, and the third size dimension, z, respectively. Therefore, the total number of independent faces identified is three and a three-dimensional morphological PB model, corresponding three parameters, x, y, z, as shown in Figure 1, can be formulated to model the morphological changes of growing potash alum crystals in aqueous solutions.[20]

Under the above assumptions, the morphological PB equation can be formulated as Eq. 6 below[20]:

$$\frac{1}{V_T(t)}\frac{\partial}{\partial t}[\psi(x,y,z,t)V_T(t)] + \frac{\partial}{\partial x}[G_1(x,t)\psi(x,y,z,t)] + \frac{\partial}{\partial y}[G_2(y,t)\psi(x,y,z,t)] + \frac{\partial}{\partial z}[G_3(z,t)\psi(x,y,z,t)] = R(t) \tag{6}$$

where ψ is the number population density function in the suspension at time, t, G_1, G_2, and G_3 are the growth rates of faces {111}, {100}, and {110}, respectively, V_T is the total volume of the suspension in a reactor, and R is the number of crystals generated by secondary nucleation in the reactor. The first term on the left-hand side in Eq. 6 is the accumulation term of population. The second, third and fourth terms are the population changes for the three main habit faces, respectively, due to crystal growth in the corresponding directions.

The growth rates of three faces {111}, {100}, and {110} for potash alum crystals can be estimated from literature[2,25,34] with the following equations[20]:

$$G_1 = 7.753 \times 10^{-7}\sigma_{\text{eff},1}^{1.5} \tag{7}$$

$$G_2 = 1.744 \times 10^{-6}\sigma_{\text{eff},2}^{1.5} \tag{8}$$

$$G_3 = 1.124 \times 10^{-6}\sigma_{\text{eff},3}^{1.5} \tag{9}$$

where $\sigma_{\text{eff},1}$, $\sigma_{\text{eff},2}$, and $\sigma_{\text{eff},3}$ are the effective relative supersaturation of faces {111}, {100}, and {110}. For potash alum crystals with three dominant habit faces, {111}, {110}, and {100}, experiments indicated that only two faces, {100} and {110}, demonstrated GRD.[1,2,28] Therefore, $\sigma_{\text{eff},1}$ in Eq. 7 will be the normal relative supersaturation, σ, of potash alum solution as used in.[20] However, in here, $\sigma_{\text{eff},2}$ and $\sigma_{\text{eff},3}$ in Eqs. 8 and 9 will be estimated using Eq. 4 with an equivalent edge length. Two methods could be used. The first method which was employed in this study is to use the shortest edge lengths of faces {100} and {110} for the estimation of the equivalent edge length, L^*. The corresponding equivalent edge lengths for faces {100} and {110} can be estimated by the following equations:

$$L_{100}^* = \min\{2(x-\sqrt{2}z), \sqrt{2}(\sqrt{3}-2)x - \sqrt{2}y + 4z\} \tag{10}$$

$$L_{110}^* = \min\{2(x-\sqrt{2}z), \sqrt{2}(1-\sqrt{3})x + 2\sqrt{2}y - 2z\} \tag{11}$$

The second method was compared with the first, but not finally adopted. It defines the equivalent edge length, L^*, of a cube using the total surface area of a habit face, i.e., for {100} face

$$L_{100}^* = \sqrt{\frac{A_{100}}{6}} = \sqrt{2[(\sqrt{3}x-y)^2 - 4(\sqrt{6}/2x - z)^2]} \tag{12}$$

where L_{100}^* is the equivalent edge length of face {100} and A_{100} is the total surface area of this face. By replacing L in Eq. 4 with the new edge length, L_{100}^*, the effective relative supersaturation and the corresponding growth rate distributions of {100} face can be calculated using Eq. 8. Similarly an equivalent edge length for {110} face, L_{110}^*, can be estimated with

$$L_{110}^* = \sqrt{\frac{A_{110}}{12}} = \sqrt{(\sqrt{6}x - 2z)[(2\sqrt{2}+\sqrt{6})y - \sqrt{6}x - 2z]} \tag{13}$$

and the corresponding effective relative supersaturation and growth rate calculated. Computational results obtained with this method will be compared with those using the first method.

Yokota et al.[35] presented a method for estimating the kinetic parameters of crystal growth and secondary nucleation for batch cooling crystallisation of potash alum. Based on the obtained parameters, the nucleation term, $R(t)$, in Eq. 6 can be estimated by the following equation[35]:

$$R(t) = 5.4 \times 10^{16}\overline{G}^2 C_s M_s \tag{14}$$

where $\overline{G}$ is the averaged value from crystal growth rates in all three directions, M_s is the molecular weight of solid, and C_s, the solid concentration in unit volume of suspension in a well-mixed batch crystallizer, can be calculated by $\rho_s/M_s \int_x \int_y \int_z V_c \cdot \psi(x,y,z,t)dx\,dy\,dz$.

The morphological PB Eq. 6, together with the growth rate Eqs. 7–9 and mass balance in a reactor, was solved using a discretisation method, moment of classes, which is an extension of the numerical solution procedure for a two-dimensional PB equation described in David et al.[36] and Puel et al.[13] The method of moment of classes[13,20,36] will be described briefly in the next paragraph, but here it is worth noting that there are alternative approaches published in literature.[37–43] For example, the method of characteristics provides an elegant solution approach for reducing the PB equation to an ordinary differential equations by finding characteristic curves in the crystal size-time plane.[42,38] For the current study of modeling crystal growth with GRD effect, however, the method of characteristics requires that the growth rate be rewritten as a product of time-dependent and

size-dependent parts,[42] which turns out to be difficult to achieve. Other techniques worth investigation for solving morphological population balance equations with GRD include higher resolution discretisation schemes,[11,38] method of lines,[33] generalized finite-element scheme,[37] moving grid technique,[40] hierarchical solution strategy based on multilevel discretisation,[41,43] and the cell-ensemble method.[39] Investigation of these algorithms is obviously important when the effects of agglomeration, breakage, secondary nucleation etc. need to be taken into account.

The three-dimensional size domain was discretized into n_1, n_2, n_3 classes. The corresponding size and characteristic dimensional length of each class in each dimension are $\Delta x_i = x_i - x_{i-1}$, $\Delta y_j = y_j - y_{j-1}$, $\Delta z_k = z_k - z_{k-1}$ and $\bar{x}_i = (x_{i-1} + x_i)/2$, $\bar{y}_j = (y_{j-1} + y_j)/2$, $\bar{z}_k = (z_{k-1} + z_k)/2$, respectively. Therefore, a system of $n_1 \times n_2 \times n_3$ three-dimensional classes was formed with the class $Cl_{i,j,k}$, being delimited by (x_i, x_{i-1}), (y_j, y_{j-1}), (z_k, z_{k-1}) and a set of $n_1 \times n_2 \times n_3$ ordinary differential equations can be formed by integrating Eq. 6 over class $Cl_{i,j,k}$ of x, y, and z:

$$\frac{1}{V_T(t)}\frac{d}{dt}\left[N_{i,j,k}(t)V_T(t)\right] + \left[FX^O_{i,j,k}(t) - FX^I_{i,j,k}(t)\right] + \left[FY^O_{i,j,k}(t) - FY^I_{i,j,k}(t)\right] + \left[FZ^O_{i,j,k}(t) - FZ^I_{i,j,k}(t)\right] = R_{1,1,1}(t) \quad (15)$$

where $N_{i,j,k}(t)$ is the number of crystals in the class $Cl_{i,j,k}$:

$$N_{i,j,k}(t) = \int_{x_{i-1}}^{x_i}\int_{y_{j-1}}^{y_j}\int_{z_{k-1}}^{z_k} \psi(x,y,z,t)\,dx\,dy\,dz \quad (16)$$

and the first term on the left hand side of Eq. 15 is the accumulation term and the second term is the net flow of crystals in class $Cl_{i,j,k}$ in x direction with the superscripts, O and I, denoting the crystal flowing outletting from and inletting into the $Cl_{i,j,k}$ class:

$$FX^O_{i,j,k}(t) - FX^I_{i,j,k}(t) = G_1(\bar{x}_i, t)\left[a_i N_{i,j,k}(t) + b_i N_{i+1,j,k}(t)\right] - G_1(\bar{x}_{i-1}, t)\left[a_{i-1} N_{i-1,j,k}(t) + b_{i-1} N_{i,j,k}(t)\right] \quad (17)$$

where $a_i = \Delta x_{i+1}/[\Delta x_i(\Delta x_{i+1}+\Delta x_i)]$ and $b_i = \Delta x_i/[\Delta x_{i+1}(\Delta x_{i+1}+\Delta x_i)]$. Similarly, the third and fourth terms on the left hand side of Eq. 15 are the net flows of crystals in class $Cl_{i,j,k}$ in y and z directions, which can be estimated in the similar way. By assuming that the size of nuclei is within the smallest class, the $R(t)$ in Eq. 6 will have nonzero value only in this class, i.e., $R(t) = R_{1,1,1}(t)$. The boundary conditions for crystal flow fluxes are:

$$FX^I_{1,j,k}(t) = FY^I_{i,1,k}(t) = FZ^I_{i,j,1}(t) = 0 \quad (18)$$

$$FX^O_{1,j,k}(t) = FY^O_{i,1,k}(t) = FZ^O_{i,j,1}(t) = 0 \quad (19)$$

With negligible effect of crystallisation and temperature variation on total volume, the volume of suspension, $V_T(t)$, can be calculated by $V(0)/[1 - M_s/\rho_s\, C_s(t)]$, and the solute concentration, $C(t)$, can be estimated with $C(0) - C_S(t)/[1 - M_s/\rho_s\, C_s(t)]$.

The discretised population balance equations (Eq. 15), together with a Guassian-type initial population distribution and the boundary conditions (Eqs. 18 and 19) under the assumption of negligible secondary nucleation (i.e., $R(t) = 0$), were solved in the mesh ranges of 0~18, 0~27, and 0~25 μm in x, y, and z directions, respectively, with the number of the size classes being $100 \times 100 \times 100$ and the corresponding mesh width being $0.18 \times 0.27 \times 0.25$ μm. The generated one million discretised population balance equations in ordinary differential form were solved simultaneously using the Runge-Kutta-Fehlbergh 4th/5th order solver[44] with automatic time-step control and the criteria of the absolute and relative tolerance being 10^{-6} and 10^{-4}, respectively. A moving mesh technique was applied during the calculation when the mean values of the normal distances (x, y, z) were propagated a few meshes from their starting locations. Test runs with either larger number of size classes, hence smaller corresponding mesh width, or smaller absolute and relative tolerance produced similar prediction. For simulation with secondary nucleation as well as GRD, the moving mesh technique was not used due to the generation of nuclei in the smallest class. The mesh ranges in x, y and z directions were 0~36, 0~35, and 0~33 μm, respectively, with the number of the size classes being $200 \times 130 \times 130$ and the same mesh widths as before.

The obtained growth of individual faces, {111}, {100}, and {110}, will be used to reconstruct[20] potash alum crystal shape at different crystallisation time stages and subsequently to estimate crystal properties such as shape distribution, mean size distribution, and surface area changes of each face.

Hot-Stage Experiment

An on-line imaging system that has been used in our previous studies[45–49] for monitoring crystallisation in batch stirred tank reactors is used here to monitor crystallisation of potash alum in a Linkam heating and freezing stage (LTS350)[50] (Figure 4). The hot-stage has an area of 40 × 40 mm for the sample and a platinum resistor embedded

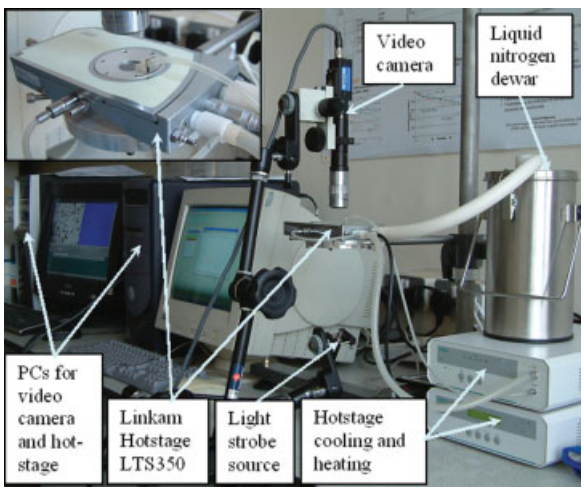

Figure 4. A Linkam hot-stage for crystallisation monitored by a real-time digital video microscopy system for the measurement of shape evolution of potash alum crystals.

[Color figure can be viewed in the online issue, which is available at www.interscience.wiley.com.]

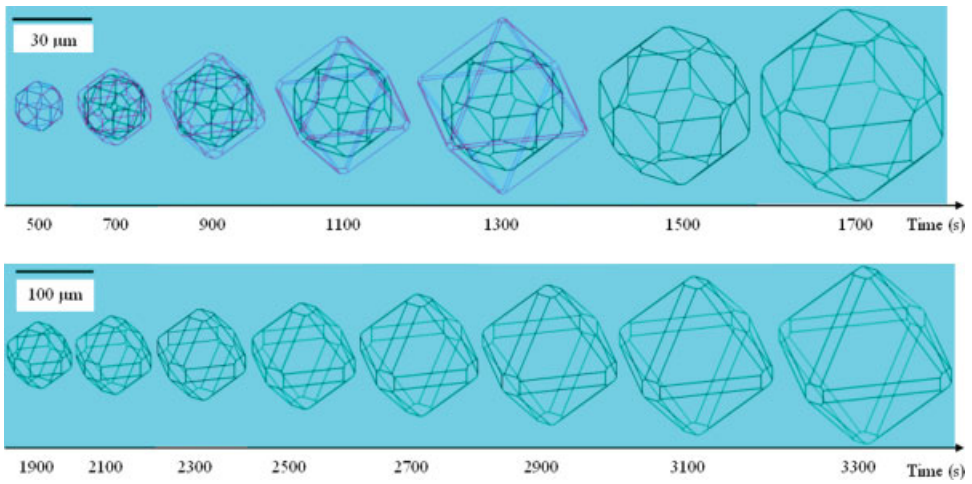

Figure 5. Comparisons of crystal shape evolution during crystallisation process of potash alum crystals.

(Magenta—GRD excluded in morphological PB modeling; Black—growth rates of faces {100} and {110} affected by crystal boundary strain and/or dislocations).

close to the surface of the sample for accurate temperature recording. The light aperture is small (2.5 mm Φ) in order to minimize the temperature gradient across the sample. The sample chamber has valves for the control of the environment surrounding the sample. The sample temperature is controlled by a temperature controller (CI94) with a working temperature range of −196–350°C and temperature stability of 0.1°C. Liquid nitrogen is used for cooling experiments. Details of the on-line imaging system can be found in the previous publications,[45–49] and of the Linkam hot-stage from the company's website.[50] Saturated solution (at 40°C saturation temperature) was prepared with 23.7 g of potash alum in 100 ml of fresh distilled water. The hot-stage was maintained at 40°C for over half an hour with an empty sample holder. Then a few drops of the saturated solution were injected into the sample holder and the hot-stage system was cooled down from 40°C to 30°C with a constant cooling rate. The on-line image acquisition has a maximum frequency of up to 30 images per second with a pixel resolution of 640 × 480. A xenon stroboscopic light source was used for illumination with a fiber optic guide to conduct the light. The captured image frames were sent to a PC running Video Savant® software[51] for storage and display.

Results and Discussions

Crystal growth modeling with GRD

This section focuses discussion on modeling the growth of the crystal population in the reactor under the effect of GRD, without inclusion of breakage, agglomeration, and secondary nucleation. Breakage and agglomeration are not included in the simulation since for potash alum crystals, the complex inorganic hydrate displays no known cleavage planes for particle fracture. Strongly bonded equant particle morphology is not particularly known for attrition. The crystal chemistry for all crystal habit faces displays an intimate mixture of cation, anion and hydrating water molecules in such a manner that significant particle/particle agglomeration is not expected. Exclusion of secondary nucleation is also expected to not causing significant effect on the results, since the simulation was carried out under relatively low supersaturation level, a condition that is known to be able to minimize secondary nucleation therefore the growth of seeds dominate the process. This point will be further discussed in the next sub-section when secondary nucleation estimation will be introduced into the model.

Figure 5 shows the comparisons of modeled crystal shape evolution during crystallization of potash alum crystals under a constant cooling rate of 0.05°C/min with and without the inclusion of GRD in the growth rates of faces {100} and {110}. Noting that when the effect of GRD on the growth rates of faces {100} and {110} is incorporated into morphological PB calculations, unless specified, the value of the mosaic spread angle is 1.1° and the equivalent edge lengths for faces {100} and {110} are their corresponding shortest edge lengths. It is clear that the fast growing face {100}, which might be due to water inclusion,[1] will eventually vanish completely if the GRD effect is not included in the morphological PB calculations (see the crystals colored in magenta in Figure 5). However, when the GRD effect is included, the boundary strain and/or dislocations affect the effective growth rates of both faces, {100} and {110}, i.e., slowing down their growth rates. Therefore, the crystals, colored in black in Figure 5, can continuously grow with all three habit faces from a few microns to 100 μm or more.

Figure 6 shows the size distributions of individual faces at different time instants during crystallisation with and without taking into account the GRD effect. It can be seen that the shape of size distributions for both cases is kept being Gaussian-type. The peak values of the population showed no obvious change during crystallization with the full width of half maximum being kept constant. At the 500th s, all faces have similar perpendicular distances from the crystal geometric center. However, at the 1100th s, the normal distance to the {111} face from the geometric center of the crystal was two times longer, while the normal distances to the {100} and {110} faces have changed from about 9 μm to around 29 and 22 μm, i.e., about 3.2 and 2.4 times respectively,

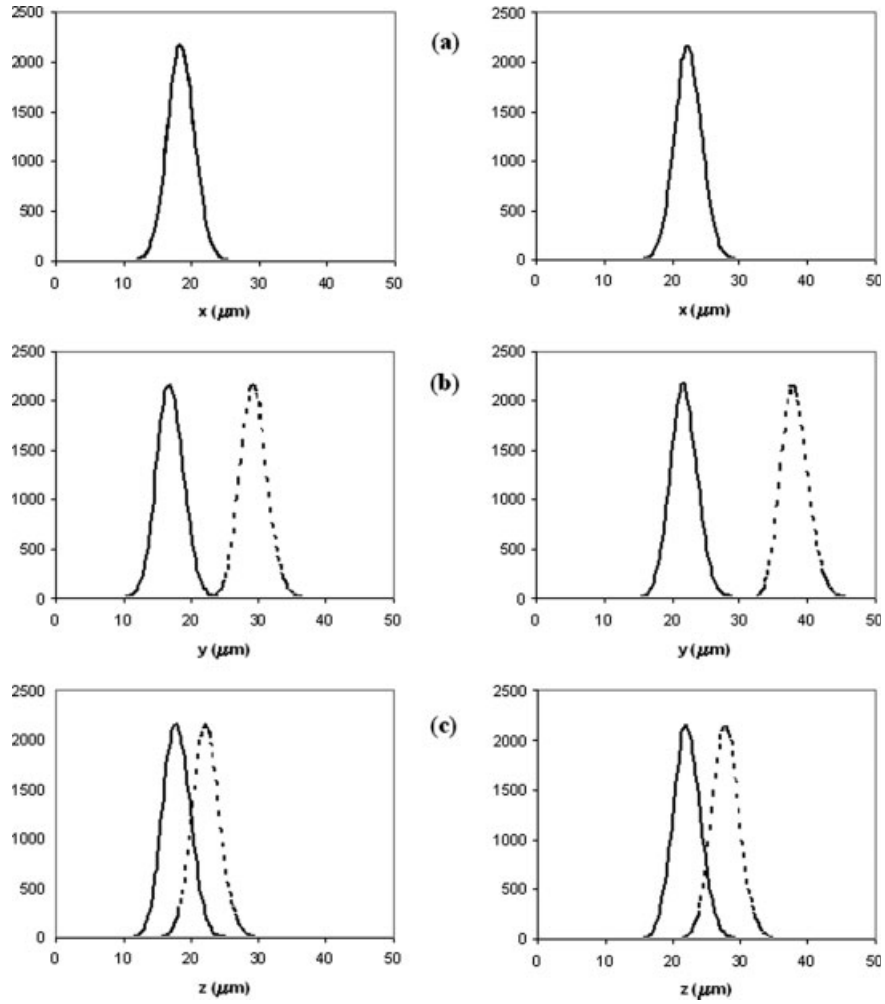

Figure 6. Size distributions of individual faces during crystallization (Solid curves—PB modeling results with GRD effect; dotted curves—PB modeling results without GRD effect).

The three plots in the left and right columns represent PB modeling results at 1100 and 1300 s, respectively. (a) size distributions for {111} face, i.e., *x* axis; (b) size distributions for {100} face, i.e., *y* axis; and (c) size distributions for {110} face, i.e., *z* axis.

when the GRD effect is not included in the morphological PB modeling. However, with the inclusion of the GRD effect, the increase of the two normal distances to the faces {100} and {110} is very similar to that of the normal distance to the {111} face. The predicted results using the morphological PB modeling with GRD effect also shows that, at the 3300th s, the normal distances of the three individual faces, {111}, {100}, and {110}, are 85.9, 125.7, and 98.6 μm, respectively.

The variations of crystal growth rates of three individual faces {111}, {100}, and {110} are illustrated in Figure 7 for both cases, with and without considering GRD. The growth rates of face {111} for both cases are completely the same due to the fact that no GRD effect was applied to that face. However, the growth rates of the other two faces have been reduced as a result of the inclusion of the GRD effect in the simulation. It is interesting to note that the decrease and increase of the growth rate of face {100} in a serial repeating order, as shown in Figure 7, may be caused by boundary strain[1,2] and water inclusion,[1] respectively. The corresponding normal distances of individual faces of potash alum crys-

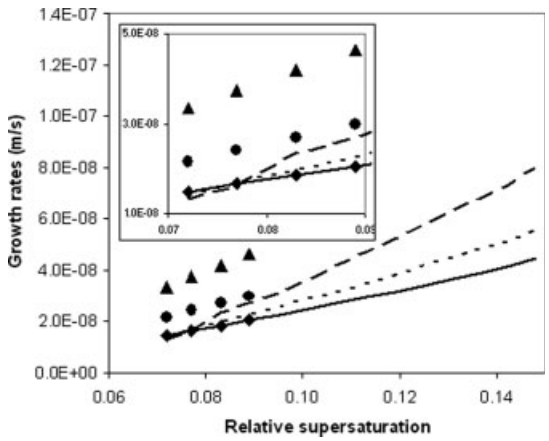

Figure 7. Effect of crystal growth strain (dislocation) on growth rates of three individual faces of potash alum crystals.

(Growth rates without GRD effect: diamonds – face {111}, triangles – face {100}, circles – face {110}; Growth rates with GRD effect: thick solid line – face {111}, thick dashed line – face {100}, thick dotted line – face {110}).

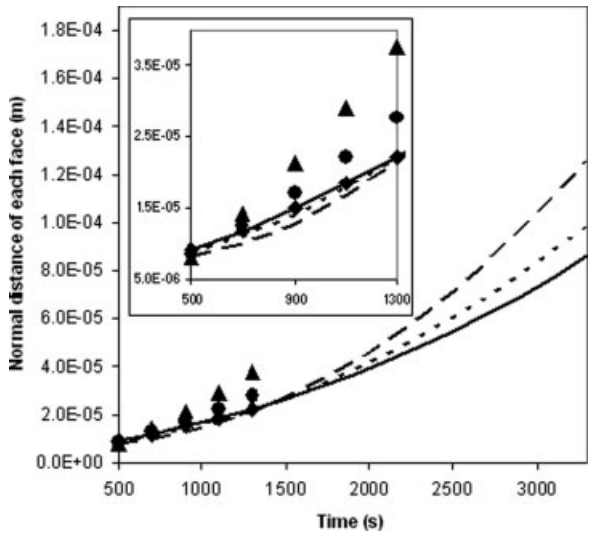

Figure 8. Effect of crystal growth strain (dislocation) on the growth of three individual faces of potash alum crystals. (symbol notations are as same as in Figure 7).

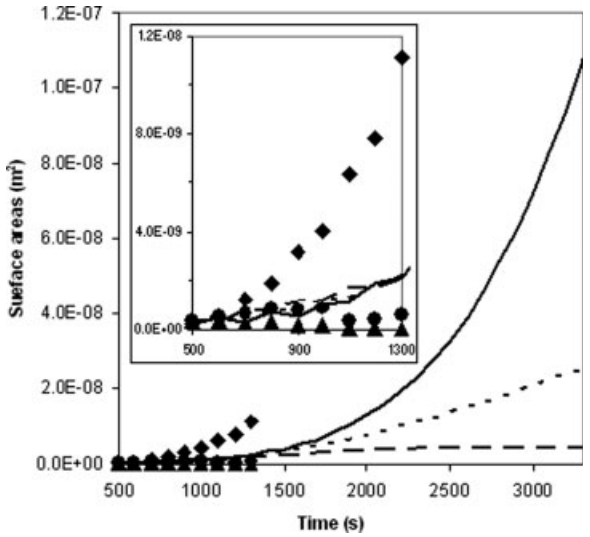

Figure 10. Surface area changes of three individual faces {111}, {100}, and {110} of potash alum crystals during crystallization with and without including the effect of crystal growth strain on growth rates (symbol notations are as same as in Figure 7).

tals are plotted in Figure 8. The normal distances of faces {100} and {110} from the morphological PB prediction with the GRD effect show lower values, which correspond to their lower growth rates.

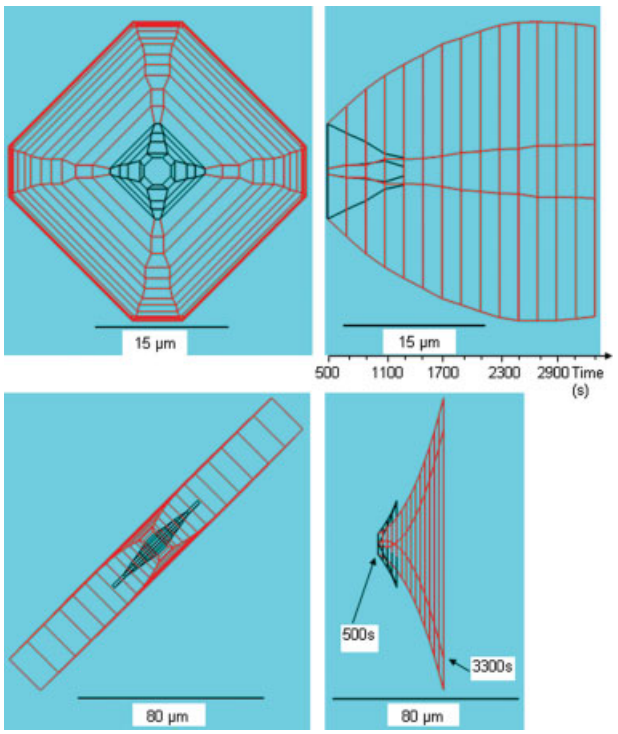

Figure 9. Evolution of individual faces of potash alum crystals during crystallisation with (red color) and without (black color) considering the effect of crystal growth strain on growth rates (top—face {100}; bottom—face {110}).

Figure 9 shows variations of faces {100} and {110} during crystallization with and without taking into account the effect of crystal boundary strain on growth rates. It is clear that the predicted surface evolution of face {100} without considering the GRD effect indicates a trend towards complete disappearance of this face. However, when the GRD effect is considered to this face, its surface enlarges with time at varied speeds. Similar findings can be obtained for the surface of

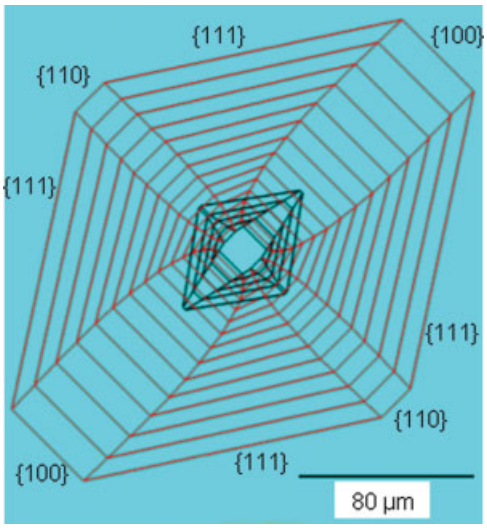

Figure 11. Growth sector boundaries of a typical potash alum crystal predicted by the morphological PB modeling with (colored in red) and without (colored in black) including the effect of crystal growth strain on growth rates.

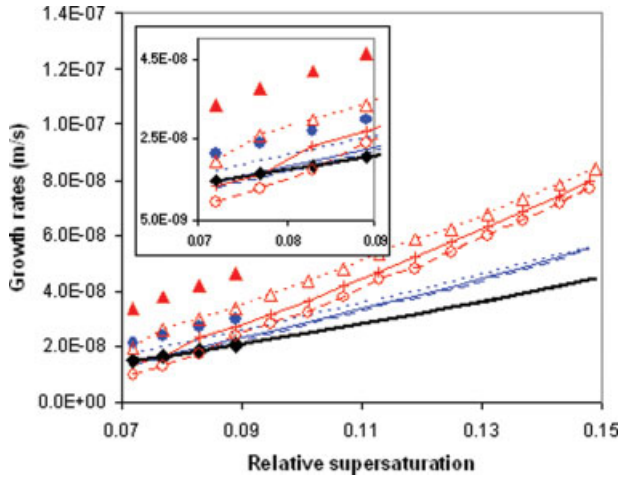

Figure 12. Effect of crystal growth strain (dislocation) on growth rates of two individual faces of potash alum crystals with different values of spread angle.

η (Growth rates without GRD effect: diamonds, face {111}; triangles, face {100}; circles, face {110}; Growth rates with GRD effect: dotted lines, solid lines and dashed lines – η = 0.5, 1.1, and 1.5, respectively; thick lines, face {111}; thin lines with symbols, face {100}; thin lines, face {110}). [Color figure can be viewed in the online issue, which is available at www.interscience.wiley.com.]

face {110}. The corresponding surface areas of the three faces {111}, {100}, and {110} have been illustrated in Figure 10. The surface areas of faces {100} and {110} did steadily increase with time when the GRD effect was included in the morphological PB modeling. In contrast, the corresponding surface areas became smaller and smaller until the faces reach their disappearance if the GRD effect was not used in the PB prediction.

Growth sector boundaries of a typical potash alum crystal from the calculations of morphological PB modeling with and without considering the effect of crystal boundary strain on growth rates are plotted in Figure 11. The faces {100} and {110} clearly tend to disappear completely if the GRD effect was not included in the calculations. The result would be of pure octahedral, diamond-like shape, as illustrated in Figure 6. However, when GRD is considered, all three habit faces showed continuously grow at variable speeds, which is close to that found in most experiments.[1–3,5]

Figures 12 and 13 show the effect of crystal boundary strain (dislocation) on the growth rates and normal distances of two individual faces, {100} and {110}, with different values of crystal lattice spread angle, η, respectively. The growth rate of face {111} did not include the GRD effect, a condition corresponds to a spread angle of zero, hence no difference was found between the four calculations using the morphological PB modeling (η = 0.0, 0.5, 1.1, 1.5). However, with the increase of the spread angle, the growth rates of faces {100} and {110} steadily decrease with faster reduction of growth rate for the face {100}. Similar findings can be obtained for the variations of normal distances of the three habit faces as shown in Figure 13. It can be seen from Figure 12 that the magnitude of the decrease and increase of growth rate of face {100} is bigger than that of face {110}. As shown in Figure 14, the surface area of face {100} tends to be constant or increase with the increase of time when the spread angle is 1.1° or 1.5°. On the other hand, the trend of the surface area of face {100} with the spread angle of 0.5° indicates that the face might disappear eventually. Similar findings can be found for the change of the surface area of the face {110}.

Figures 15 and 16 show the growth rates and the corresponding growth of the three individual faces, {111}, {100}, and {110}, using the value of mosaic spread angle of 1.1° but two different methods for the estimation of the equivalent edge lengths for faces {100} and {110}, i.e., the shortest

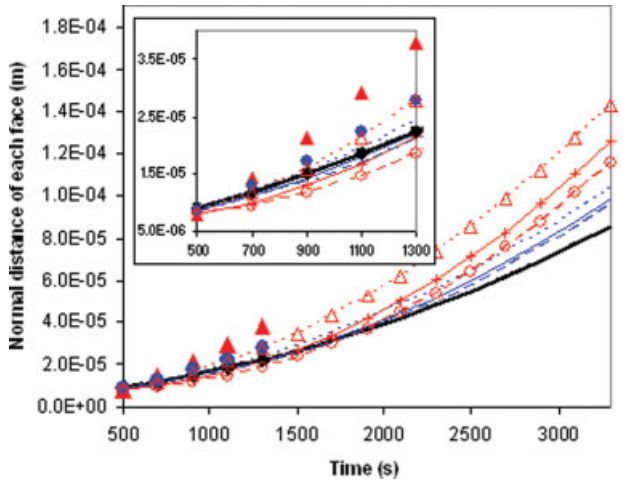

Figure 13. Effect of crystal growth strain (dislocation) on the growth of two individual faces of potash alum crystals with different values of spread angle.

η (symbol notations are as same as in Figure 12). [Color figure can be viewed in the online issue, which is available at www.interscience.wiley.com.]

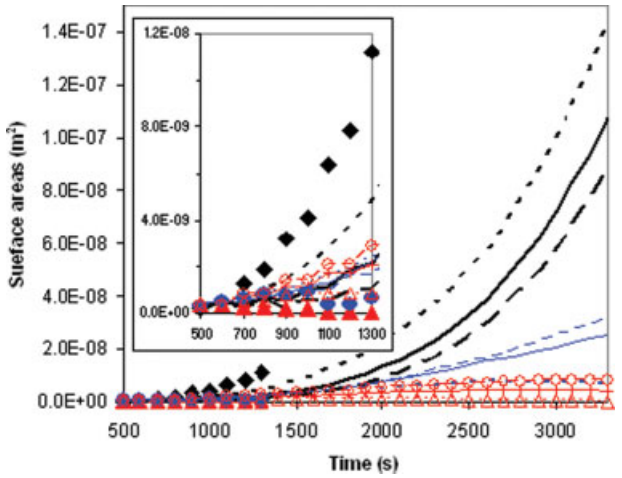

Figure 14. Effect of crystal growth strain (dislocation) on the surface area variations of two individual faces of potash alum crystals with different values of spread angle.

η (symbol notations are as same as in Figure 12). [Color figure can be viewed in the online issue, which is available at www.interscience.wiley.com.]

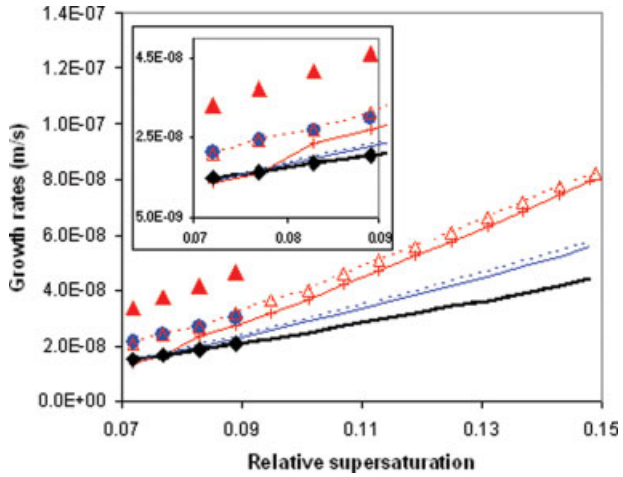

Figure 15. Effect of crystal growth strain (dislocation) on growth rates of two individual faces of potash alum crystals with different methods for the calculations of the equivalent edge lengths, L^*_{100} and L^*_{110}.

(Growth rates without GRD effect: diamonds, face {111}; triangles, face {100}; circles, face {110}; Growth rates with GRD effect: dotted lines, L^*_{100} and L^*_{110} calculated by Eqs. 12 and 13; solid lines, L^*_{100} and L^*_{110} equal to the corresponding shortest edge lengths (Eqs. 10 and 11); thick lines, face {111}; thin lines with symbols, face {100}; thin lines, face {110}). [Color figure can be viewed in the online issue, which is available at www.interscience.wiley.com.]

edge lengths or calculation with Eqs. 12 and 13. The corresponding comparisons of surface areas of the three faces are plotted in Figure 17. It can be seen that much less variations of the growth rate of face {100} with crystallization time occurred with the use of the second method for the estimation of the equivalent edge lengths (Figure 15). The growth rate for the face {100} obtained using the second method for L^*_{100} is significantly higher than that using the first method for the calculation of L^*_{100}. However, the growth rates of face {110} in both cases have similar values. Accordingly, the growth of the normal distance of face {100} with the second method was faster (Figure 16), hence resulting in smaller surface area (Figure 17), whereas the normal distance and surface area of face {110} have similar values for both methods. By comparing Figures 12–14 with Figures 15–17, it can be seen that the growth rates, normal distances and surface areas of the three faces obtained using the second method for the estimation of L^*_{100} and L^*_{110} with the mosaic spread angle of 1.1° are very similar to those using the first method but with the mosaic spread angle of 0.5°.

Figure 18 shows the comparisons of potash alum crystal shape obtained from hot-stage experiments and the morphological PB modeling with a constant cooling rate of 3°C/min using the first method of the estimation of L^*_{100} and L^*_{110} and a spread angle of 1.1°. It can be seen that the crystal shape obtained from the morphological PB modeling with the GRD effect and hot-stage experiments is generally compatible to each other. The hot-stage experiments did not produce potash alum crystals with pure octahedral, diamond-like shape (see Figures 5 and 18), is an indication that the GRD mechanism has played a role. In order to compare the shape of potash alum crystals between prediction and experiments in details, the on-line images were recorded using the digital video microscope system in the transmission mode. The obtained images were taken from a view perpendicular to the face {111}. Therefore, the area of the parallel surfaces of face {111} was recorded on the images as white area (see the a-b-c-d-e-f area in Figures 18b1 ~ b3 and c1 ~ c3). The predicted shape using the morphological PB model with and

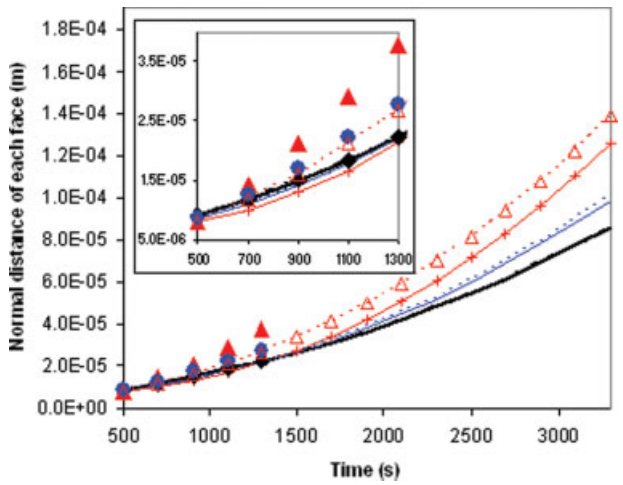

Figure 16. Effect of crystal growth strain (dislocation) on the growth of two individual faces of potash alum crystals with different methods for the calculations of the equivalent edge lengths, L^*_{100} and L^*_{110} (symbol notations are as same as in Figure 15).

[Color figure can be viewed in the online issue, which is available at www.interscience.wiley.com.]

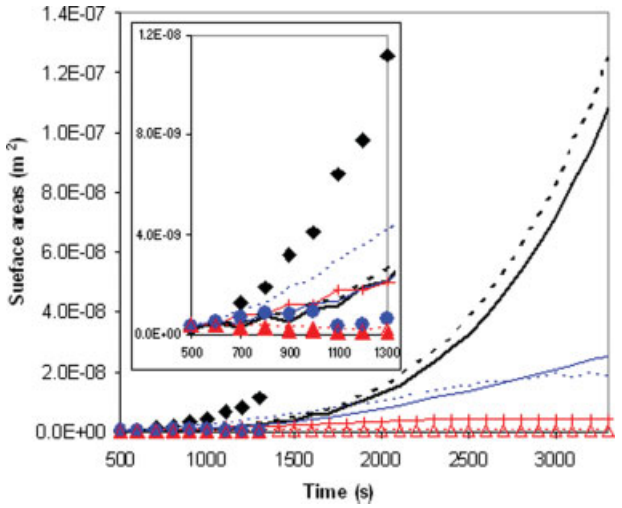

Figure 17. Effect of crystal growth strain (dislocation) on the surface area variations of two individual faces of potash alum crystals with different methods for the calculations of the equivalent edge lengths, L^*_{100} and L^*_{110} (symbol notations are as same as in Figure 15).

[Color figure can be viewed in the online issue, which is available at www.interscience.wiley.com.]

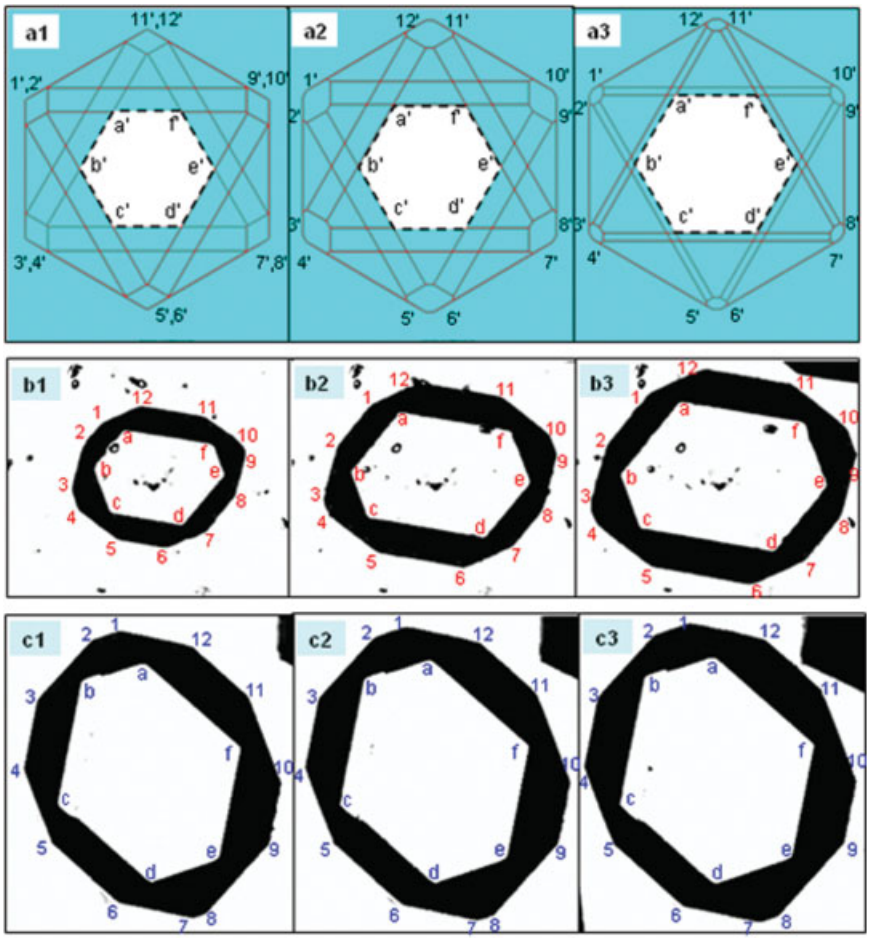

Figure 18. Crystal shape obtained from morphological PB modeling with cooling rate of 3°C/min.

(a1, without the GRD effect at the 200th s; a2, with the GRD effect at the 200th s; a3, with the GRD effect at the 240th s) and images obtained form hot-stage experiments (b1, b2, and b3—80th, 100th, and 120th s with cooling rate of 5°C/min; c1, c2, and c3—200th, 240th, and 280th s with cooling rate of 3°C/min). [Color figure can be viewed in the online issue, which is available at www.interscience.wiley.com.]

without the GRD effect was also viewed at the same angle with the corresponding white area of face {111} being defined by a′-b′-c′-d′-e′-f′ (Figures 18a1 ~ a3). The other areas of potash alum crystals were recorded on the images as black color (Figures 18b1 ~ b3 and c1 ~ c3) due to the diffraction of the xenon stroboscopic light passing through the angled surfaces. From that particular viewpoint, the recorded image of potash alum crystals has twelve edges which are defined by numbers 1 ~ 12 in Figures 18b1 ~ b3 and c1 ~ c3. Similarly the twelve edges obtained from the morphological PB modeling are identified by numbers 1′ ~ 12′ as shown in Figures 18a1 ~ a3. However, the crystal shape obtained from the PB calculation without the GRD effect at the 200th s only has six edges due to that the shortest edges of face {100} were reaching the point of complete disappearance. Although the area sizes and the edge lengths between the images from hot-stage experiments and the crystal shape predicted using the morphological PB modeling with the GRD effect are not exactly the same, generally speaking, the crystal shape at the 240th s obtained using the morphological PB modeling with the GRD effect is in reasonably good agreement with the on-line images taken from the hot-stage experiments using the digital video microscopy system.

Crystal growth modeling with secondary nucleation and GRD

In this section, secondary nucleation is added into the morphological population balance modeling, and its effect on crystal growth is discussed. The kinetic parameters of secondary nucleation for batch cooling crystallization of potash alum was estimated using the method in literature,[35] and presented in Eq. 14. The literature model was based on the traditional definition of particle size, i.e., volume equivalent diameters of spheres; here we made an assumption that the secondary nuclei have similar shape as the seeds. Because of the small size of nuclei,[52] it is also acceptable to assume that all nuclei generated from the secondary nucleation will be within the smallest class, i.e., about 0.2 μm of normal distances in x, y, and z directions, which are compatible to the critical size of nuclei discussed in literature.[52]

Figure 19 shows the results of the growing crystals of the seeds, and of the nuclei at different time instants. Comparing the size distributions of three individual faces, {111}, {100}, and {110}, it is interesting to notice that the effect of secondary nucleation on the growth of seeded crystals is not significant. This can be attributed to the fact that the nuclei generated from secondary nucleation are small in crystal size[52] (x, y, and

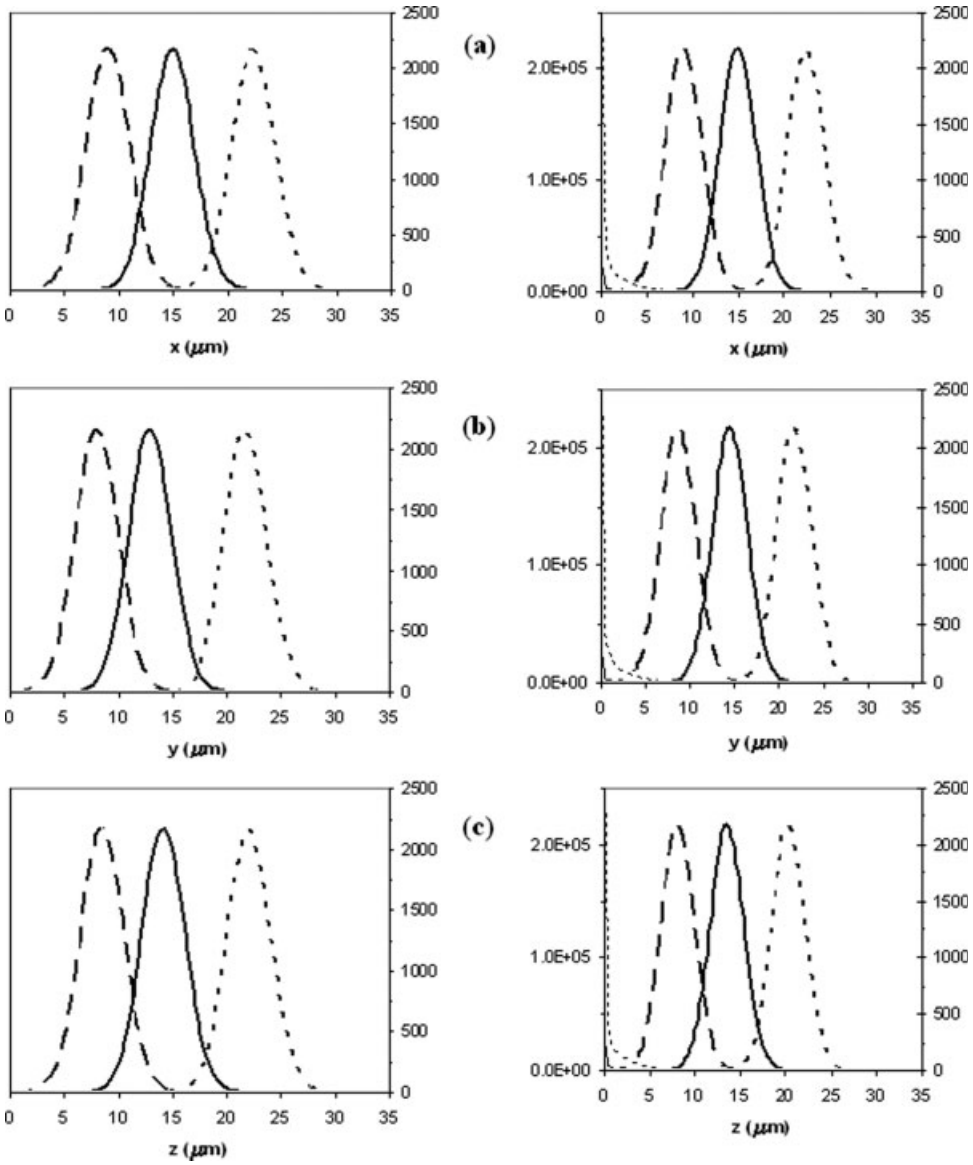

Figure 19. Size distributions of individual faces during crystallization (Thin curves, crystals generated from secondary nucleation with scale on the left axis; thick dashed curves, 500 s; thick solid curves, 900 s; thick dotted curves, 1300 s).

The three plots in the left column represent PB modeling results with GRD effect but no secondary nucleation, the three plots in the right column considered both GRD and secondary nucleation. (a) size distributions for {111} face, i.e., x axis; (b) size distributions for {100} face, i.e., y axis; and (c) size distributions for {110} face, i.e., z axis.

z for nuclei ≈ 0.2 μm), leading to changes in supersaturation that is not large enough to give noticeable impact on the process of growth of seeds. In addition, as indicated by Figure 3, small crystals, i.e., here the nuclei grew at much lower rates than large crystals i.e., the seeds. However, as a result of secondary nucleation, the particle size distribution was changed from mono-modal to bimodal. The results were found to be consistent with experimental results from Yokota et al.[35]

Concluding Remarks

Crystal GRD is known to be responsible for many sophisticated crystal structures. This article has introduced GRD into a newly developed morphological PB model for crystallization. The predicted results for potash alum show clearly the effect of GRD on the shape evolution for potash alum crystals, crystal growth rates of two faces {100} and {110}, and the variations of the corresponding surface areas. The growth rate variations of face {100} indicate that the boundary strain (dislocation) did cause growth rate reduction and the water inclusion onto the face {100} may be the reason for growth rate increase. The crystal shape obtained from the morphological PB modeling with GRD was shown to be compatible to that grown from solution in hot-stage experiments, while if GRD was not considered, the morphological PB model predicted potash alum crystals with pure octahedral, diamond-like shape, which were not produced by the hot-stage experiments.

Acknowledgments

The work presented in this article is funded by the UK Engineering and Physical Sciences Research Council (EPSRC) (Grant references: EP/C009541 and EP/E045707). Thanks are also due to Prof Kevin J Roberts for useful discussions on crystal growth rate dispersion. We also would like to thank the industrial collaborators for the two EPSRC projects: AstraZeneca (Dr Gerry Steele and Dr Mike J. Quayle), Malvern Instruments (Dr Richard J Tweedie, Mr Andy Prior and Mr Duncan Roberts), Nexia Solutions (Dr Dominic Rhodes), Pfizer (Dr Rado Penchev, Dr Ivan Marziano and Professor Robert Docherty), Syngeta (Dr Neil George) and 3M Health Care (Dr Chris Blatchford). The sponsorship of Malvern Instruments for the University of Leeds—Malvern Partnership *IntelliSense* (www.intellisense.org.uk) is gratefully acknowledged.

Notation

A_{100}, A_{110} = surface area of {100} and {110} faces (m^2)
A_{gb} = grain boundary area (m^2)
a, b, c = unitcell parameters (length) (Å)
a_i, b_i = coefficient (m^{-1})
b^* = length of the Burgers' vector (m)
C = solute concentration (mol m^{-3})
C^* = solubility (mol m^{-3})
$Cl_{i,j,k}$ = three-dimensional class
C_S = concentration of solid in the suspension (mol m^{-3})
dx,dy,dz = differential distances in x, y, z directions (m)
E = energy per particle (N m)
$FX_{i,j,k}$, $FY_{i,j,k}$, $FZ_{i,j,k}$ = net flow rate of crystals in class $Cl_{i,j,k}$ in x, y, and z directions ([nb] m^{-3} s^{-1})
G = crystal growth rate (m s^{-1})
$\bar{G}$ = averaged crystal growth rate (m s^{-1})
G_1, G_2, G_3 = growth rate of faces {111}, {100}, and {110} (m s^{-1})
Gs = shear module (N m^{-2})
k = Boltzmann constant (J K^{-1})
k_0 = growth kinetic coefficient (m s^{-1})
L = crystal edge length (m)
L^* = equivalent crystal edge length (m)
L^*_{100},L^*_{110} = equivalent edge length of faces {100} and {110} (m)
l_m = edge length of mosaic block (m)
M_s = molecular weight of solid (kg mol^{-1})
$N_{i,j,k}$ = number of crystals in the class $CL_{i,j,k}$ ([nb] m^{-3})
n = growth power
n_1, n_2, n_3 = number of classes in x, y and z directions
R = number of crystals generated from secondary nucleation ([nb] m^{-3} s^{-1})
r_c = radius of the dislocation center (m)
t = time (s)
T = solution temperature (K)
V = volume of solution (m^3)
V_c = volume of crystals (m^3)
V_T = total volume of suspension (m^3)
x, y, z = Cartesian coordinates (m)
x_i, y_j, z_k = discretized characteristic parameters of crystal (m)
$\bar{x}_i, \bar{y}_j, \bar{z}_k$ = characteristic parameters of class CL_i, CL_j, and CL_k (m)

Greek letters

α, β, γ = unitcell parameters (angle) (°)
$\Delta x_i,\Delta y_j,\Delta z_k$ = extent of classes CL_i, CL_j and CL_k (m)
γ_{gb} = grain boundary tension (N m^{-1})
η = mosaic spread angle (°)
ν = Poisson's ratio
θ = mosaic block angle (°)
ρ_s = density of solid (kg m^{-3})
σ = relative supersaturation ($= C/C^* - 1$)
σ_{eff} = effective relative supersaturation
$\sigma_{eff,1}$,$\sigma_{eff,2}$,$\sigma_{eff,3}$ = effective relative supersaturation of faces {111}, {100}, and {110}
Ω = molecular volume (m^3)
ψ = number population density function in the suspension ([nb] m^{-3} m^{-3})

Literature Cited

1. Klapper H, Becker RA, Schmiemann D, Faber A. Growth-sector boundaries and growth-rate dispersion in potassium alum crystals. *Cryst. Res. Technol.* 2002;37:747–757.
2. Ristic RI, Shekunov B, Sherwood JN. Long and short period growth rate variations in potash alum crystals. *J. Cryst. Growth* 1996;160:330–336.
3. van der Heijden AEDM, van der Eerden JP. Growth rate dispersion: the role of lattice strain. *J. Cryst. Growth* 1992;118:14–26.
4. Garside J, Phillips VR, Shah MB. Size-dependent crystal-growth. *Ind. Eng. Chem. Fundam.* 1976;15:230–233.
5. Lacmann R, Herden A, Mayer C. Kinetics of nucleation and crystal growth. *Chem. Eng. Technol.* 1999;22:279–289.
6. Matsuoka M, Abe Y, Uchida H, Takiyama H. Mechanism of growth rate enhancement by micro-crystals for the potash alum-water system. *Chem. Eng. Sci.* 2001;56:2325–2334.
7. Mullin JW, Garside J. Crystallization of aluminium potassium sulphate—a study in assessment of crystallizer design data. I. Single crystal growth rates. *Trans. Inst. Chem. Eng. Chem. Eng.* 1967;45: T285–T290.
8. Ristic RI, Sherwood JN, Shripathi T. Strain variation in the (100) growth sectors of potash alum single-crystals and its relationship to growth-rate dispersion. *J. Cryst. Growth* 1990;102:245–248.
9. Briesen H. Simulation of crystal size and shape by means of a reduced two-dimensional population balance model. *Chem. Eng. Sci.* 2006;61:104–112.
10. Ma CY, Wang XZ, Roberts KJ. Multi-dimensional population balance modelling of the growth of rod-like L-glutamic acid crystals using growth rates estimated from in-process imaging. *Adv. Powder Technol.* 2007;18:707–723.
11. Ma DL, Tafti DK, Braatz RD. High-resolution simulation of multidimensional crystal growth. *Ind. Eng. Chem. Res.* 2002;41:6217–6223.
12. Oullion M, Puel F, Fevotte G, Righini S, Carvin P. Industrial batch crystallization of a plate-like organic product. In situ monitoring and 2D-CSD modelling. II. Kinetic modelling and identification. *Chem. Eng. Sci.* 2007;62:833–845.
13. Puel F, Fevotte G, Klein JP. Simulation and analysis of industrial crystallization processes through multidimensional population balance equations. I. A resolution algorithm based on the method of classes. *Chem. Eng. Sci.* 2003;58:3715–3727.
14. Puel F, Fevotte G, Klein JP. Simulation and analysis of industrial crystallization processes through multidimensional population balance equations. II. A study of semi-batch crystallization. *Chem. Eng. Sci.* 2003;58:3729–3740.
15. Zhang YC, Doherty MF. Simultaneous prediction of crystal shape and size for solution crystallization. *AIChE J.* 2004;50:2101–2112.
16. Gadewar SB, Doherty MF. A dynamic model for evolution of crystal shape. *J. Cryst. Growth* 2004;267:239–250.
17. Zhang YC, Sizemore JP, Doherty MF. Shape evolution of 3-dimensional faceted crystals. *AIChE J.* 2006;52:1906–1915.
18. Snyder RC, Doherty MF. Faceted crystal shape evolution during dissolution or growth. *AIChE J.* 2007;53:1337–1348.
19. Snyder RC, Studener S, Doherty MF. Manipulation of crystal shape by cycles of growth and dissolution. *AIChE J.* 2007;53:1510–1517.
20. Ma CY, Wang XZ, Roberts KJ. Morphological population balance for modelling crystal growth in individual face directions. *AIChE J.* 2008;54:209–222.
21. Amara N, Ratsimba B, Wilhelm A, Delmas H. Growth rate of potash alum crystals: comparison of silent and ultrasonic conditions. *Ultrason. Sonochem.* 2004;11:17–21.
22. Bravais MA. Études Cristallographiques [Crystallographic studies]. Paris: Gauthier–Villars; 1866.
23. Donnay J, Harker D. A new law of crystal morphology extending the Law of Bravais. *Am. Mineral.* 1937;22:446–467.
24. Friedel M. Etudes sur la loi de bravais. *Bull. Soc. Franc Miner.* 1907;9:326.
25. Nollet S, Hilgers C, Urai JL. Experimental study of polycrystal growth from an advecting supersaturated fluid in a model fracture. *Geofluids* 2006;6:185–200.

26. Brunsteiner M, Price SL. Surface structure of a complex inorganic crystal in aqueous solution from classical molecular simulation. *J. Phys. Chem. B* 2004;108:12537–12546.
27. Read WT, Shockley W. Dislocation models of crystal grain boundaries. *Phys. Rev.* 1950;78:275–289.
28. Ristic RI, Shekunov BY, Sherwood JN. The influence of synchrotron radiation-induced strain on the growth and dissolution of brittle and ductile materials. *J. Cryst. Growth* 1997;179:205–212.
29. Sherwood JN, Ristic RI. The influence of mechanical stress on the growth and dissolution of crystals. *Chem. Eng. Sci.* 2001;56:2267–2280.
30. Jones CM, Larson MA. Using dislocations and integral strain to model the growth rates of secondary nuclei. *Chem. Eng. Sci.* 2000;55: 2563–2570.
31. Burton WK, Cabrera N, Frank FC. The growth of crystals and the equilibrium structure of their surfaces. *Philos. Trans. R. Soc. Lond.* 1951;243:299–358.
32. Garside J, Davey RJ. Secondary contact nucleation—kinetics, growth and scale-up. *Chem. Eng. Commun.* 1980;4:393–424.
33. Gerstlauer A, Mitrovic A, Motz S, Gilles ED. A population model for crystallization processes using two independent particle properties. *Chem. Eng. Sci.* 2001;56:2553–2565.
34. Matsuoka M, Kamada T, Takiyama H. Growth rate enhancement of potash alum crystals by microcrystals. *J. Cryst. Growth* 1996;158: 322–327.
35. Yokota M, Sato A, Kubota N. A simple method for evaluating kinetic parameters in non-isothermal batch crystallization. *Chem. Eng. Sci.* 2000;55:717–722.
36. David R, Marchal P, Marcant B. Modeling of agglomeration in industrial crystallization from solution. *Chem. Eng. Technol.* 1995; 18:302–309.
37. Gerstlauer A, Gahn C, Zhou H, Rauls M, Schreiber M. Application of population balances in the chemical industry—current status and future needs. *Chem. Eng. Sci.* 2006;61:205–217.
38. Gunawan R, Fusman I, Braatz RD. High resolution algorithms for multidimensional population balance equations. *AIChE J.* 2004;50: 2738–2749.
39. Henson MA. Cell ensemble modeling of metabolic oscillations in continuous yeast cultures. *Comput. Chem. Eng.* 2005;29:645–661.
40. Kumar S, Ramkrishna D. On the solution of population balance equations by discretization. III. Nucleation, growth and aggregation of particles. *Chem. Eng. Sci.* 1997;52:4659–4679.
41. Pinto MA, Immanuel CD, Doyle FJ. A feasible solution technique for higher-dimensional population balance models. *Comput. Chem. Eng.* 2007;31:1242–1256.
42. Sotowa KI, Naito K, Kano M, Hasebe S, Hashimoto I. Application of the method of characteristics to crystallizer simulation and comparison with finite difference for controller performance evaluation. *J. Process Control* 2000;10:203–208.
43. Sun NF, Immanuel CD. Efficient solution of population balance models employing a hierarchical solution strategy based on a multilevel discretization. *Trans. Inst. Meas. Control* 2005;27:347–366.
44. Shampine LF, Watts HA. Subroutine RKF45. In: Forsythe GE, Malcolm MA, Moler CB, editors. *Computer Methods for Mathematical Computations*. Englewood Cliffs, N.J.: Prentice-Hall, 1977:135–147.
45. Calderon De Anda J, Wang XZ, Lai X, Roberts KJ. Classifying organic crystals via in-process image analysis and the use of monitoring charts to follow polymorphic and morphological changes. *J. Process Control* 2005;15:785–797.
46. Calderon de Anda J, Wang XZ, Lai X, Roberts KJ, Jennings KH, Wilkinson MJ, Watson D, Roberts D. Real-time product morphology monitoring in crystallization using imaging technique. *AIChE J.* 2005;51:1406–1414.
47. Wang XZ, Calderon De Anda J, Roberts KJ. Real-time measurement of the growth rates of individual crystal facets using imaging and image analysis: a feasibility study on needle-shaped crystals of L-glutamic acid. *Chem. Eng. Res. Des.* 2007;85A:921–927.
48. Wang XZ, Calderon De Anda J, Roberts KJ, Li RF, Thomson GB, White G. Advances in on-line monitoring and control of the morphological and polymorphic forms of organic crystals grown from solution (paper downloadable from www.kona.org.jp/html/about/index2005.html). *KONA.* 2005;23:69–85.
49. Wang XZ, Roberts KJ, Ma CY. Crystal growth measurement using 2D and 3D imaging and the perspectives for shape control. *Chem. Eng. Sci.* 2008;63:1171–1184.
50. Linkam Scientific Instruments. Available at: http://www.linkam.co. uk/.
51. IO Industries. Available at: http://www.ioindustries.com/vs.htm.
52. Yau ST, Vekilov PG. Quasi-planar nucleus structure in apoferritin crystallization. *Nature*. 2000;406:494–497.

Appendix

This appendix provides additional information of the computational details used in the simulations.

Initial conditions

A Gaussian-type crystal PB distribution was used to initialize the distribution of seeds:

$$N_{1,1,1} = A_0 \exp\left\{-2\left[\left(\frac{x-x_0}{\sigma_x}\right)^2+\left(\frac{y-y_0}{\sigma_y}\right)^2+\left(\frac{z-z_0}{\sigma_z}\right)^2\right]\right\} \tag{A1}$$

where the mean values of seeded crystals, x_0, y_0, and z_0, were 9, 8, and 8.5 μm, respectively. Their corresponding standard deviations, σ_x, σ_y, and σ_z, were 4 μm. The constant, A_0, for the simulation can be obtained through mass balance calculation of potash alum crystals (2200 in this study).

Boundary conditions

It was assumed that there was no crystals and solution passing through the boundaries in three individual face directions (x, y, and z) (see Eqs. 18 and 19).

Parameters

The crystallization started at 500 s with the suspension temperature of 38°C and relative supersaturation level of 0.0659 under a cooling rate of 0.05°C/min. The mesh sizes for the x, y, and z were 0.18, 0.27, and 0.25 μm, respectively, with their corresponding numbers of classes being 100, 100, and 100 for simulations excluding secondary nucleation with moving mesh technique or 200, 130, 130 for simulations including secondary nucleation with fixed mesh distribution. The corresponding seeds concentration was 0.0649 mol/m^3. The Runge-Kutta-Fehlbergh 4th/5th order solver with automatic time-step control was used to solve the PB equation with the criteria of the absolute and relative tolerance being 10^{-6} and 10^{-4}, respectively.

Manuscript received Oct. 29, 2007, and revision received Apr. 14, 2008.